Size-dependent properties of $YBa_2Cu_3O_{6+x}$ nanopowder

2003 J. Phys.: Condens. Matter 15 2103

(http://iopscience.iop.org/0953-8984/15/12/327)

INSTITUTE OF PHYSICS PUBLISHING JOURNAL OF PHYSICS: CONDENSED MATTER

J. Phys.: Condens. Matter **15** (2003) 2103–2114 PII: S0953-8984(03)57459-8

Size-dependent properties of $YBa_2Cu_3O_{6+x}$ nanopowder

P Paturi, J Raittila, H Huhtinen, V-P Huhtala and R Laiho

Wihuri Physical Laboratory, Department of Physics, University of Turku, FIN-20014 Turku, Finland

Received 17 December 2002
Published 17 March 2003
Online at stacks.iop.org/JPhysCM/15/2103

Abstract

$YBa_2Cu_3O_{6+x}$ nanopowder, prepared by the citrate sol–gel method, is segregated by sedimentation in ethanol into three size groups with average particle heights of 0.7, 1.6 and 2.3 nm. The structural properties and composition of the powders, investigated by x-ray diffraction, atomic force microscopy, Auger electron spectroscopy and EPR-spectroscopy, show no clear differences, except the size. According to investigations by magnetometry and by non-resonant microwave absorption the as-prepared powder contains weak links which, however, disappear during the segregation. The magnetic susceptibility of the samples decreases with the decreasing particle size, in agreement with the susceptibility values calculated from the London equations for cylindrical particles smaller than the London penetration depth. In all three size groups the critical temperature of superconductivity is 92 K.

1. Introduction

The superconductivity of high-temperature superconductors (HTS) is essentially associated with the CuO_2-layers in the crystal structure [1–3]. Investigations of ultra-thin $YBa_2Cu_3O_{6+x}$ (YBCO) films have shown that, when the thickness of the film is decreased the zero-resistance transition temperature $T_{c,0}$ decreases and the transition width increases [2–7]. The broadening of the transition has been attributed to unbound vortex–antivortex pairs induced in the films above the Kosterlitz–Thouless transition [5, 6]. The depression of $T_{c,0}$ has been explained by insufficient coupling between the CuO_2-layers [2]. The observation that one unit cell thickness is the lower limit for superconductivity in ultra-thin films [3] gives support to this assumption. The onset temperature of the transition, $T_{c,onset}$, is not lowered as much as $T_{c,0}$ [3] and seems to be sample-dependent [2–5]. On the other hand, no degradation of $T_{c,onset}$ was observed in $[(Ba_{0.9}, Nd_{0.1})CuO_2]_m/[CaCuO_2]_2$ superlattices with decreasing m [8] or when the buffer layer between the substrate and the YBCO film was specially chosen [9].

Mesoscopic particles of classical superconductors exhibit interesting behaviour not observed in macroscopic samples [10–12]. This poses the problem of whether nanometre-size

YBCO particles have properties different from those of ultra-thin films, where two dimensions are macroscopic. If the depression of $T_{c,onset}$ in ultra-thin films is due to insufficient interlayer coupling, it should also be observed in thin nanosize particles. But if the depression is due to sample quality or the extreme 2D nature of the films, the particles with radii of the same scale as the London penetration depth synthesized in optimum conditions might not have depressed $T_{c,onset}$.

Using magnetic methods the onset of the superconducting transition can be observed in nanosize particles, where direct resistivity measurements are impossible. In this paper we investigate YBCO nanopowders [13, 14] segregated into three size groups by sedimentation. The properties of the groups are analysed using x-ray diffraction (XRD), Auger electron spectroscopy (AES) and atomic force microscopy (AFM). The size dependence of the magnetic properties is investigated by SQUID magnetometry and non-resonant microwave absorption. Similar measurements have been done earlier for micron-sized powders [15–18] indicating a clear size dependence for critical current density, magnetization and microwave absorption. Finally the results are compared to the susceptibility calculated for cylindrical particles smaller than the London penetration depth.

2. Sample preparation and characterization

Nanosize YBCO powder was prepared by the sol–gel method where the chelating agent was citric acid. Water solutions of Y, Ba and Cu nitrates were mixed in the ratio of 1:2:3 and then citric acid ($4n(\text{citricacid}) = n(Y^{3+})$) was added to the solution. Under constant stirring ethyldiamine was added until the pH of the solution was 6. Gelation was achieved by evaporating water from the solution at 80 °C. Then the gel was fired at 500 °C for 2 h in air to obtain the precursor powder for further heat treatments.

The precursor was calcined at 790 °C for 16 h in flowing O_2 and then cooled rapidly to room temperature. After light grinding the powder was annealed at 760 °C for 24 h in a flowing Ar atmosphere and cooled at the rate of 25 °C h^{-1} to room temperature in a flowing O_2 atmosphere. In all the treatments the pressure of the flowing gas was 1 atm. The annealing was repeated three times to obtain the original powder (O) [14].

The segregation into different size groups was made by sedimentation in pure ethanol. First about 25 mg of the O-powder was added to 5 ml of ethanol and the mixture was kept in an ultrasonic bath for an hour to break up any agglomerates. Then the mixture was carefully pipetted on top of 75 ml of ethanol in a decanter glass where the biggest particles (L group) sank to the bottom. After waiting for 5 min the top part of the ethanol was removed to another decanter glass, where it was sedimented for 3 h (M group). The smallest particles (S group) were obtained when the top layer was again removed and left to evaporate. There is no essential difference in the time which the S, M and L particles were kept in ethanol. It is also emphasized that no mechanical grinding that could cause strains in the grains took place during the preparation and segregation.

The distributions of the particle sizes in the S, M and L groups were determined with AFM measurements and scanning electron microscopy (SEM). Typical AFM images are shown in figure 1. To obtain the samples for AFM and SEM a small amount of powder was mixed with ethanol in an ultrasonic bath. Then a drop of this mixture was pipetted onto a (100) Si substrate placed on an ultrasonically vibrated table. During the evaporation of ethanol the particles were spread on the substrate and their sizes were subsequently measured. Since the particles are flat and almost circular, they are characterized by their height and radius. The results measured from several images for each size group are compiled in table 1, showing a clear trend in the height but much smaller relative differences in the radii. The height distributions are skewed to

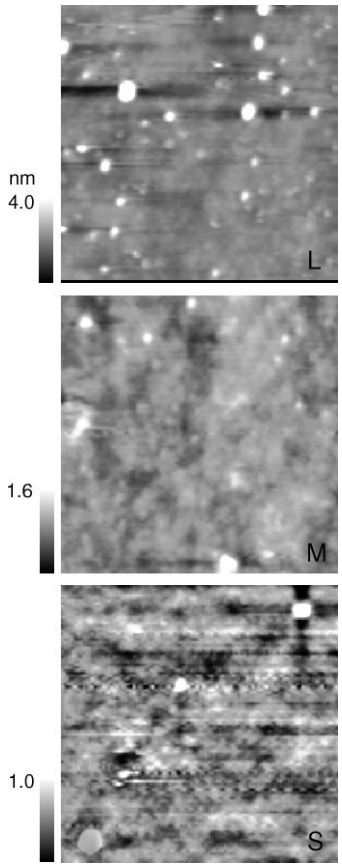

Figure 1. Typical AFM images of the particles in the segregated size groups. The area in all the images is 2 μm $\times$ 2 μm.

the right with skewness of 3.02, 3.63 and 3.65 for the S, M and L group, respectively. The radii values fall nicely on the normal distribution curve. The biggest particle found in the L sample was 18 nm high and 190 nm wide, while the biggest particle in the S sample was 6.3 nm high and 90 nm wide. The SEM images confirmed that there are no extremely large particles in the samples, but the resolution was too poor to measure the exact areas of the particles. The results from AFM are in fair agreement with the average sizes of 38, 41, 46 and 46 nm calculated from the width of the x-ray peak (113) [19] for the S-, M-, and L-powders, respectively (see figure 2).

Atomic concentrations of the samples were determined with AES using a Perkin-Elmer PHI 610 spectrometer. The base pressure in the chamber was below 10^{-9} Torr and the primary electron beam was 5 kV at 90 nA current on an area of 100 $\times$ 100 μm^2. The compositional analysis was made using the 1747, 591 and 920 eV lines for Y, Ba and Cu, respectively, and the AES sensitivity factors were determined from a ceramic high purity YBCO pellet as 0.040 (Y), 0.21 (Ba) and 0.10 (Cu). The samples were prepared by pipetting about 0.4 mg of the segregated powder dispersed in ethanol onto Si(100) substrates, as for the AFM samples. The surface of the samples had large amounts of carbon, most of which could be removed by 3 kV Ar ion sputtering. To avoid preferential sputtering of the metals in YBCO, sputtering times as short as possible (60 s) were chosen. The results of measurements averaged over

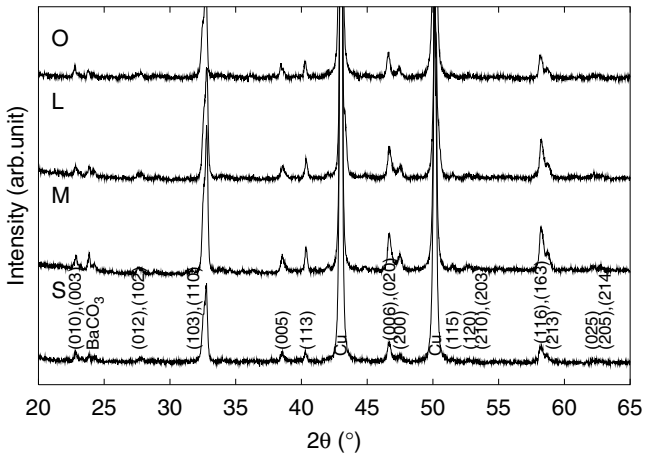

Figure 2. XRD scans of the segregated samples. The differences in peak heights are due to different sample volumes and distributions on the Si substrates. The large Cu peaks at 43° and 50° arise from the sample holder.

Table 1. Average particle sizes with standard errors and standard deviations as measured by AFM for the segregated powders. *N* is the number of analysed particles in each sample.

Sample *N*	Height (nm) StdDev (nm)	Radius (nm) StdDev (nm)
L	2.27 ± 0.05	49.4 ± 0.4
717	2.1	11.3
M	1.6 ± 0.2	56.0 ± 1.6
57	1.1	12.2
S	0.68 ± 0.05	38.0 ± 0.8
207	0.7	11.0

Table 2. Atomic concentrations of metals in the segregated samples measured by AES.

Sample (at.%)	Y	Ba	Cu
Nominal	16.67	33.33	50.0
O	17.12	29.48	53.40
L	15.49	34.71	49.80
M	16.21	30.33	53.46
S	16.94	37.04	53.40

four places on the surface for each sample are shown in table 2. All the powders are close to the nominal composition of YBCO and no trend in the concentrations can be observed. The deviations from the nominal values are within the limits of statistical variation.

The samples prepared for AES were also used for XRD analysis shown in figure 2. According to XRD measurements the O-powder has orthorhombic structure with $a = 0.3825$ nm, $b = 0.3881$ nm and $c = 1.1667$ nm. Traces of $BaCO_3$ and CuO, amounting to 6.8 and 2.4 mass%, respectively, were found in the diffraction patterns. A small wide peak due to either $BaCuO_2$ or Y_2O_3 was also present, but since no other peaks corresponding to these compounds were found definite identification was not possible. The small $BaCO_3$ peaks at ≈24°–25° appear in samples from all the size groups at approximately the same relative

intensity compared to adjacent YBCO peaks. Therefore we can see that $BaCO_3$ does not concentrate in any size group. From the analysis of the XRD pattern we can conclude that all the samples have an orthorhombic crystal structure with the same lattice parameters as the O-powder. Since the observed impurities are non-magnetic they do not contribute to the magnetic results.

3. Magnetic and microwave properties of the segregated samples

Temperature dependencies of the zero-field-cooled (ZFC) and field-cooled (FC) magnetic susceptibilities of the segregated powders measured with a SQUID magnetometer at $B = 0.5$ mT are shown in figure 3(a). The samples were prepared by pipetting about 1 ml of a mixture of segregated powder and ethanol into a small plastic tube covered inside with Teflon tape. During evaporation of the ethanol the powder was spread on the Teflon and afterwards the sample was weighed. The masses of the samples were 10–20 mg and the 9.2% contributed by the impurities was taken into account when calculating the susceptibilities. The critical temperature T_c was the same (92 K) in all the size groups. For the S and M samples the χ_{FC} and χ_{ZFC} curves are the same, which is expected for small particles where the threshold field for vortex penetration is high [20, 21]. When measured in a field of 8 mT no difference between the ZFC and the FC curves in any of the samples was found. The O and L samples have the same χ_{FC} at 5 K, which means that the superconducting properties of the powders are preserved in the sedimentation stages.

The field dependencies of the magnetizations in different samples, measured at 5 K, are shown in figure 3(b). The $M(B)$ curve of the O sample is nonlinear and, when combined with the $\chi(T)$ in figure 3(a), it is confirmed that the reason for the nonlinearity observed in weak fields are the weak links with critical temperature of 60–70 K. Careful analysis shows that the $M(B)$ curve of the L sample also has a nonlinear part for $B < 1$ mT but there are much fewer weak links than in the O sample. This is consistent with the temperature dependence of χ. The magnetizations of the S and M samples show linear field dependencies corresponding to the χ (5 K) $= -0.037$ and -0.063, respectively. The susceptibility of the L sample is estimated as -0.09.

An EPR spectrometer working at 9 GHz was used to measure non-resonant and resonant microwave absorption. For non-resonant absorption field modulations at 100 Hz and 100 kHz with amplitude of 0.1 mT were used. Therefore the signal represents the second field derivative of the absorption curve. As shown in figure 4 in the O sample the absorption has the maximum at 5 K and decreases rapidly as the temperature increases, achieving a relatively constant level at $\approx$60 K and disappearing at 90 K. In the S sample the second field derivative of the absorption is about 100 times smaller than in the O sample and the temperature dependence of the curve is similar to that of the magnetization curve. The absorption curves of the L and M samples are similar to those of the O and S samples, respectively, and for clarity they are not shown in figure 4. These data are similar to those of, for example, [13, 22] and differ from those measured without modulation [15, 23]. The difference is due to dissipation by the vortices and shielding currents created by the modulation field, which is naturally absent in non-modulated data. Recently the difference has been measured also in MgB_2 [24]. Since modulated non-resonant absorption in zero field is caused by shielding currents in the particles and the interparticle weak links [25, 26], our result in figure 4 suggests that the absorption by the weak links is much stronger than absorption by the particles. Consistent with the magnetization results the strong rise in the signal below 60 K in the O (and L) sample can be assumed to be due to weak links. Above 60 K all the absorption is due to the shielding of the particles and is much smaller than below 60 K. Presumably due to vortex jumps in the weak

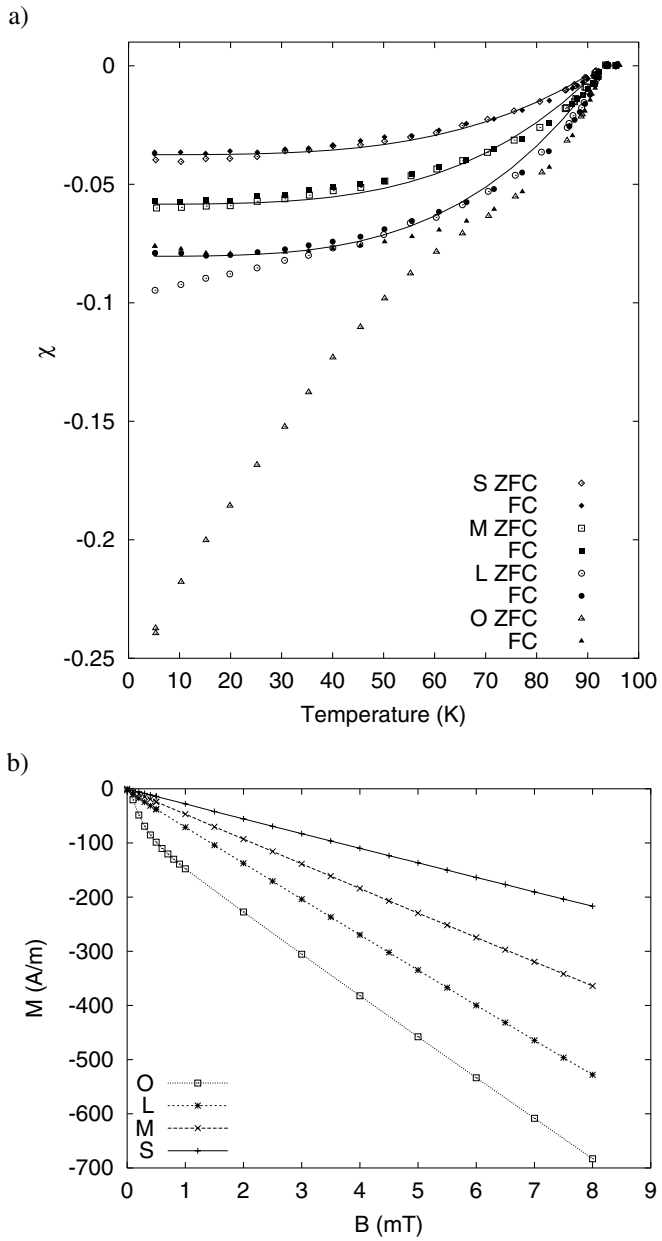

Figure 3. (a) The FC and ZFC temperature dependencies of the susceptibilities in $B = 0.5$ mT in the sedimented samples and in the original powder. The full lines are fits to equations (11) and (12). (b) The field dependence of the magnetization measured at 5 K for all the samples.

links [25] the noise in the O (and L) curve below 60 K is also much larger than in the S (and M) curve, where no weak links are present.

The resonant microwave absorption was measured using field modulation at 100 kHz and with a modulation amplitude of 0.2 mT. The EPR signal of Cu^{2+} with $g = 2.10$ was observed in all the sample groups, as shown in figure 5(a). The signal is strongest in sample S

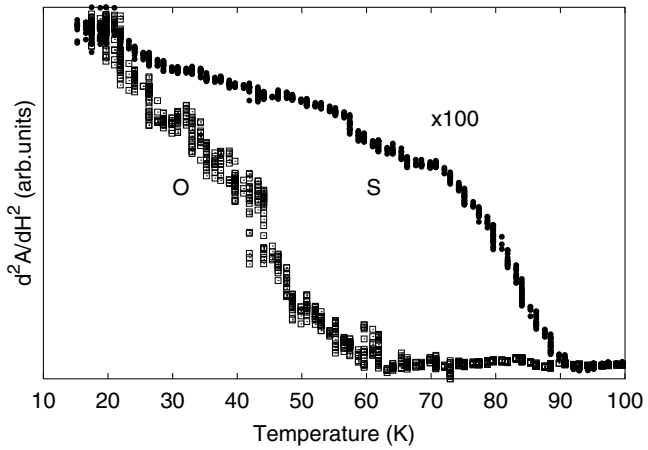

Figure 4. Temperature dependence of the second field derivative of the non-resonant microwave absorption at zero field. The scale for the S sample is multiplied by 100 to emphasize the difference between the shapes of the curves. The signal also appears at about 90 K for the O sample.

and decreases when the particle size grows. Normally EPR peaks are not seen in cuprate superconductors [27, 28], as is almost the case in the O sample. The two possibilities for observing the Cu^{2+} EPR signal in YBCO are impurities [29] and O–Cu–O chain fragments in oxygen-deficient samples [27]. Since our samples are fully oxygenated the main suspects are the impurities. The temperature dependence of the EPR line intensity in the S sample follows closely the C/T-law typical for paramagnetic materials. Among the usual impurities in YBCO, $BaCO_3$ and Y_2O_3 naturally do not give the Cu^{2+} signal and neither does CuO below its antiferromagnetic ordering temperature 230 K [30]. The EPR linewidths related to Y_2BaCuO_5 and $Y_2Cu_2O_5$ increase with decreasing temperature, contrary to our measurements [29]. $BaCuO_2$ gives an EPR signal with $g = 2.10$ [31] and the same temperature dependencies of the signal amplitude and linewidth, as observed from our sample. Thus it is fairly clear that the unidentified small XRD peak in the O powder and the Cu^{2+} EPR signal are caused by traces of $BaCuO_2$. Along with this conclusion we assume that the grain size of $BaCuO_2$ is so small that it concentrates in the S sample. This would also explain the large width of the XRD line.

4. Calculation of the susceptibility

To evaluate whether the observed small susceptibilities in the S, M and L groups are due to the small size of the particles, we calculate the susceptibilities from the London theory [32] for the size distributions measured with AFM (see table 1). The susceptibility can be expressed exactly only for some specific geometries of the sample and the magnetic field [33]. In the literature most of the numerical solutions for different geometries are given at the limit of $\lambda = 0$ [34, 35] or for thin films where two of the dimensions $\gg \lambda$ and one $\approx\lambda$ [20, 36]. Brandt has developed a method for calculating the electromagnetic response of type-II superconductors with finite λ in various geometries [37, 38], but this method is somewhat heavy for our purpose. Therefore we calculate the susceptibility of a general cylindrical particle defined by its radius R and thickness $2L$ (see figure 6(a)), assuming finite λ in all dimensions.

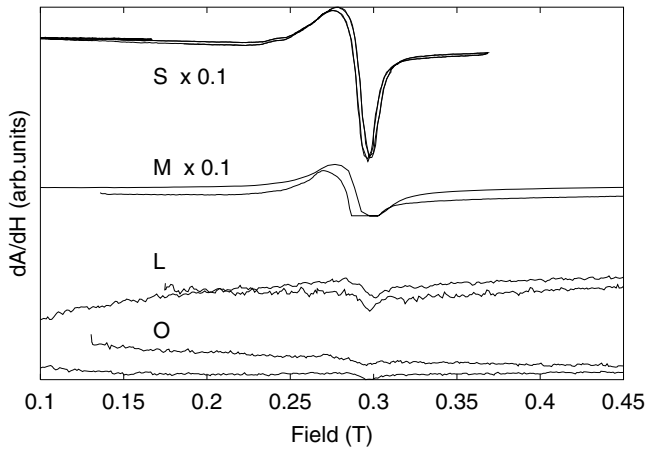

Figure 5. The EPR peak of Cu^{2+} at 15 K. The scales of the S and the M samples are multiplied by 0.1.

The current $\boldsymbol{J}$ in the cylinder is obtained from the second London equation

$$\nabla^2(\boldsymbol{\Lambda J}) = \mu_0 \boldsymbol{J}, \tag{1}$$

where $\boldsymbol{\Lambda}$ is the penetration depth tensor in cylindrical coordinates [39, p 125]:

$$\boldsymbol{\Lambda} = \begin{pmatrix} \lambda_{ab}^2 & 0 & 0 \\ 0 & \lambda_{ab}^2 & 0 \\ 0 & 0 & \lambda_c^2 \end{pmatrix} \mu_0. \tag{2}$$

For the external magnetic field $\boldsymbol{H}_0 \parallel \hat{\boldsymbol{e}}_z$ we get $\boldsymbol{J} \parallel \hat{\boldsymbol{e}}_\theta$ and solving equation (1)

$$\boldsymbol{J} = C I_1(ar) \cosh(cz) \hat{\boldsymbol{e}}_\theta, \tag{3}$$

where C is an integration constant which depends on the shape of the particle, I_1 is the modified Bessel function of the first kind of order 1 and a and c are integration constants bound by the relation

$$a^2 + c^2 = \lambda_{ab}^{-2}. \tag{4}$$

Knowing $\boldsymbol{J}$ we can calculate [39, p 124] the internal magnetic field $\boldsymbol{B}$ caused by the current from

$$\nabla \times (\boldsymbol{\Lambda J}) = -\boldsymbol{B}. \tag{5}$$

This gives

$$\boldsymbol{B} = C\mu_0 c \lambda_{ab}^2 I_1(ar) \sinh(cz) \hat{\boldsymbol{e}}_r - C\mu_0 \lambda_{ab}^2 a I_0(ar) \cosh(cz) \hat{\boldsymbol{e}}_z. \tag{6}$$

The magnetic field $\boldsymbol{M}$ caused by $\boldsymbol{J}$ is [40, p 115]

$$\boldsymbol{M}(0, 0, Z) = \frac{1}{4\pi} \int_V \frac{\boldsymbol{J} \times \hat{\boldsymbol{r}}}{r^2} \, \mathrm{d}V = \frac{1}{4\pi} \int_V \frac{C r I_1(ar) \cosh(cz)}{(r^2 + (Z - z)^2)^{3/2}} \, \mathrm{d}V \, \hat{\boldsymbol{e}}_z, \tag{7}$$

where the place of observation is at point Z on the z axis and the integration is over the volume of the cylinder. Due to cylindrical symmetry the $\boldsymbol{M} \parallel \hat{\boldsymbol{e}}_r$ component vanishes. Since we now have $\boldsymbol{M}$, $\boldsymbol{B}$ and $\boldsymbol{H}_0$, we can solve the integration constant C from

$$\boldsymbol{B}(0, 0, Z) = \mu_0(\boldsymbol{M}(0, 0, Z) + \boldsymbol{H}_0(0, 0, Z)). \tag{8}$$

Unfortunately the integral in equation (7) cannot be solved analytically, so C has to be obtained numerically.

a)

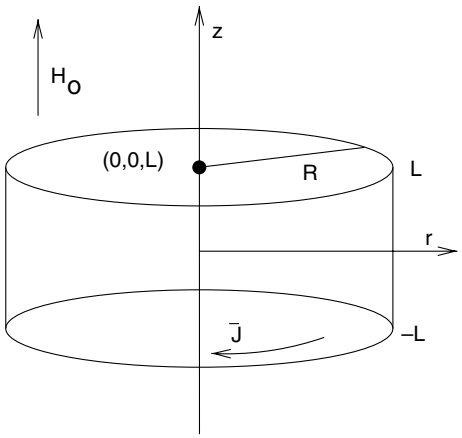

b)

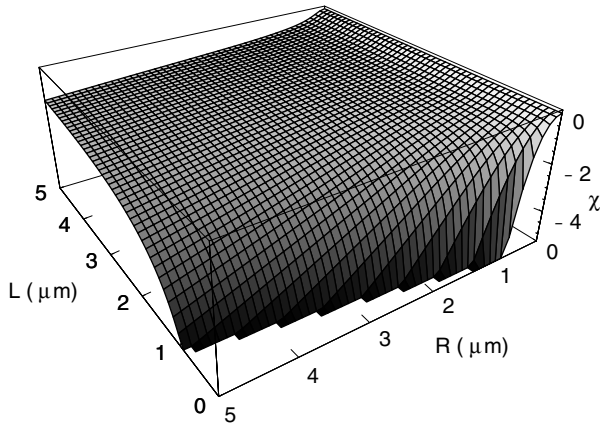

Figure 6. (a) The geometry used in the calculation of the susceptibility. $2L$ is the height and R is the radius of the cylinder. (b) The calculated susceptibility at $T = 0$ K for cylindrical particles as a function of R and L with $\lambda_{ab} = 140$ nm and $a = 0.005$ nm^{-1}.

The measurable magnetic moment $\boldsymbol{m}$ can be calculated from [40, p 119]

$$\boldsymbol{m} = \tfrac{1}{2}\int_V \boldsymbol{r} \times \boldsymbol{J}\,\mathrm{d}V \tag{9}$$

$$= -\frac{2\pi C R^2}{ac}\sinh(cL) I_2(aR)\hat{e}_z. \tag{10}$$

Solving C at the point (0, 0, L) on top of the cylinder and defining $\chi = m/(VH)$ we finally get

$$\chi = -\frac{\sinh(cL) I_2(aR)}{Lac}\left(\lambda_{ab}^2 a\cosh(cL) + \frac{1}{4\pi}\int_V \frac{r I_1(ar)\cosh(zc)}{(r^2 + (Z-z)^2)^{3/2}}\,\mathrm{d}V\right)^{-1}. \tag{11}$$

As an illustration of equation (11) the calculated values of χ are shown in figure 6(b) as a function of R and L at $T = 0$ K and with $\lambda_{ab} = 140$ nm and $a = 0.005$ nm^{-1}. When R is

Table 3. Calculated and observed susceptibilities at 5 K for different λ_{ab} [42–44] and a (in nm^{-1}) values.

	$\lambda_{ab} = 115$ nm		$\lambda_{ab} = 140$ nm		
Sample	$a = 0.001$	$a = 0.007$	$a = 0.001$	$a = 0.007$	Observed
L	−0.040	−0.040	−0.027	−0.028	−0.09
M	−0.036	−0.037	−0.024	−0.025	−0.063
S	−0.028	−0.028	−0.018	−0.019	−0.037

large and L is small, $-\chi$ becomes very large, as it should because of the large demagnetization factor of a thin film in a perpendicular magnetic field [41]. With small R and large L, $\chi(R)$ gives a parabolic curve as expected [33, p 234]. It should be noted that the demagnetization factor of the sample is built into equation (11) and that at higher temperatures, especially close to T_c, the value of λ_{ab} will increase over all the sample dimensions and the values in figure 6(b) will not hold.

Using equation (11) for the size distributions observed with AFM we get the susceptibilities shown in table 3 for different values for λ_{ab} [42–44] and the integration constant a. The calculated and observed values of χ are in good agreement, taking into account that the calculation does not contain any adjustable parameters. It can be seen that χ is fairly immune to changes of a. In particles larger than λ_{ab} the values of a and c should be known more exactly.

To take into account the random orientation of the particles the χ values in table 3 should be multiplied by $2/\pi$, because the magnetization of a flat superconducting particle is always perpendicular to the plane of the particle [45]. When the random orientation correction is taken into account the calculated values are too small by a factor of about 3. This can be explained by the mutual influence of magnetic fields generated by shielding currents in the particles. As calculated for larger particles ($\lambda \ll R, L$) by Fabbricatore *et al* [46], if the particles are distributed side by side the susceptibility is enhanced. It is more likely that the particles are side by side in the samples than that they are stacked into tall piles. This effect alone can explain the observed higher susceptibilities as compared to the calculated ones, but also AFMs preference for smaller particles may have affected the size distributions slightly.

To account for the temperature dependence of χ we write the temperature dependencies of λ_{ab} and a in the form

$$\frac{\lambda_{ab}(0)^2}{\lambda_{ab}(T)^2} = \frac{a(T)^2}{a(0)^2} = 1 - \left(\frac{T}{T_c}\right)^n, \tag{12}$$

where the exponent n describes the specific form of the $\lambda_{ab}(T)$ and $a(T)$ curves. Values between $n = 2.12$ and 4.27 with a trend of increasing n with increasing oxygen content have been measured by muon spin rotation [47]. If we insert the functions of equation (12) into equation (11) using $n = 3.5$ and calculate the $\chi(T)$ function for the size distributions S, M and L, we get the full lines in figure 3(a). The calculated values of χ are multiplied by ≈2 for easier comparison with the experimental data. In so doing we find an excellent fit in all our samples.

It should also be noted that the critical temperature is 92 K in all the size groups (see figure 3(a)). Since there are no weak links in the S and M samples and very few in the L sample, there is no possible coupling between the CuO_2 layers of different particles. This means that the depression of $T_{c,onset}$ in ultra-thin films [3–6] is more probably caused rather by the interface between the superconductor and the substrate than the reduced size of the film in one dimension.

5. Conclusions

We have prepared a YBCO nanopowder, which was segregated in ethanol into three size groups. These samples were analysed using XRD, AES, AFM and EPR and the only differences found between the groups were the particle size and concentration of $BaCuO_2$ in the smallest size group. The absolute amount of $BaCuO_2$ in the samples is too small to have any effect on their magnetizations. The magnetization and non-resonant microwave absorption of the samples show that the original powder and the particles in the largest size group contained weak links which disappeared during segregation, but that the segregation procedure did not affect the intraparticle superconducting properties. From the measurements it can be concluded that microwave absorption is an extremely sensitive probe of weak links in our nanomaterial.

The susceptibility is found to vary with the size of the particles in the samples. Starting from the London equations the susceptibility of a small cylinder (length scales less than the London penetration depth) was calculated and the results are in good agreement with the magnetic measurements. It is emphasized that the calculation did not involve any adjustable parameters and the only measured data were the size distributions of the samples. This leads us to conclude that even the smallest one unit cell thick YBCO particles are superconductive with $T_c = 92$ K and therefore the atomic structure of the unit cell is nearly perfect for the whole particle. Also the fact that $(00l)$ XRD lines can be observed supports this conclusion.

Acknowledgments

We thank Professor Leo Vlasenko for the help with the EPR measurements and Professor Kari Laajalehto for help with the Auger measurements. The Academy of Finland, the Wihuri Foundation and the Graduate School of Materials Research are acknowledged for funding this project.

References

[1] Lin J G, Huang C Y, Xue Y Y, Chu C W, Cao X W and Ho J C 1995 *Phys. Rev.* B **51** 12900
[2] Cieplak M Z, Guha S, Vadlamannati S, Giebiltowicz T and Lindenfeld P 1994 *Phys. Rev.* B **50** 12876
[3] Tang W, Ng C, Yau C and Gao J 2000 *Supercond. Sci. Technol.* **13** 580
[4] Triscone J M, Fisher O, Brunner O, Antognazza L, Kent A D and Karkut M G 1990 *Phys. Rev. Lett.* **64** 804
[5] Terashima T, Shimura K, Bando Y, Matsuda Y, Fujiyama A and Komiyama S 1991 *Phys. Rev. Lett.* **67** 1362
[6] Matsuda Y, Komiyama S, Onogi T, Terashim T, Shimura K and Bando Y 1993 *Phys. Rev.* B **48** 10498
[7] Goodrich R G, Adams P W, Lowndes D H and Norton D P 1997 *Phys. Rev.* B **56** R14299
[8] Balestrino G, Lavanga S, Medalgia P G, Origiani P and Tebano A 2001 *Phys. Rev.* B **64** 020506
[9] Grekhov I, Baydakova M, Borevich V, Davydov V, Delimova L, Liniichuk I and Lyublinsky A 1997 *Physica* C **276** 18
[10] Geim A K, Grigorieva I V, Dubonos S V, Lok J G S, Maan J C, Filippov A E and Peeters F M 1997 *Nature* **390** 259
[11] Deo P S, Schweigert V, Peeters F and Geim A 1997 *Physica* E **1** 297
[12] Deo P S, Schweigert V A, Peeters F M and Geim A K 1997 *Phys. Rev. Lett.* **79** 4653
[13] Blinov E, Fleisher V G, Huhtinen H, Laiho R, Lähderanta E, Paturi P, Stepanov Y P and Vlasenko L 1997 *Supercond. Sci. Technol.* **10** 818
[14] Raittila J, Huhtinen H, Paturi P and Stepanov Y P 2002 *Physica* C **371** 90
[15] Gould A, Jackson E, Renouard K, Crittenden R, Bhagat S, Spencer N, Dolhert L and Wormsbecher R 1988 *Physica* C **156** 555
[16] Shimizu E and Ito D 1989 *Phys. Rev.* B **39** 2921
[17] Kuwabara M and Shimooka H 1989 *Appl. Phys. Lett.* **55** 2781
[18] Babic E, Prester M, Drobac D, Marohnic Z, Nozar P, Stastny P, Matacotta F C and Bernik S 1992 *Phys. Rev.* B **45** 913
[19] Cullity B D 1978 *Elements of X-Ray Diffraction* 2nd edn (Reading, MA: Addison-Wesley) p 102

[20] Fetter A L 1980 *Phys. Rev. Lett.* **22** 1200
[21] Fleisher V G, Laiho R, Lähderanta E, Stepanov Y P and Traito K B 1996 *Physica* C **272** 26
[22] Topacli C and Harris E A 1997 *J. Phys.: Condens. Matter* **9** 1267
[23] Manheimer M A, Lofland S, Gould A, Bhagat S M, Halsey B, Green S M and Tyagi S 1991 *Physica* C **183** 324
[24] Lofland S E, Tyagi S D, Ramanujachary K V and Botsford M 2002 *Physica* C **379** 27
[25] Endo T and Yan H 1994 *Japan. J. Appl. Phys.* **33** 103
[26] Harris E A, Loftus D J, McLeish T C B and Ward P J 1991 *Supercond. Sci. Technol.* **4** 359
[27] Sichelschmidt J, Elschner B, Loidl A and Kochelaev B I 1995 *Phys. Rev.* B **51** 14
[28] Singh R J, Sharma P K, Singh A and Khan S 2001 *Physica* C **356** 285
[29] Genossar J, Shaltiel D, Zevin V, Grayevsky A and Fisher G 1989 *J. Phys.: Condens. Matter* **1** 9471
[30] Muraleedharan K and Rao T K G 1990 *J. Magn. Magn. Mater.* **89** L277
[31] Azzoni C B, Paleari A, Parravicini G B, Samoggia G, Parmigiani F and Scagliotti M 1989 *Phys. Lett.* A **139** 411
[32] London F and London H 1935 *Physica* **2** 341
[33] Shoenberg D 1952 *Superconductivity* (Cambridge: Cambridge University Press)
[34] Prozorov R, Giannetta R W, Carrington A and Araujo-Moreira F M 2000 *Phys. Rev.* B **62** 115
[35] Sanchez A and Navau C 2001 *Phys. Rev.* B **64** 214506
[36] Clem J R and Sanchez A 1994 *Phys. Rev.* B **50** 9355
[37] Brandt E H 2002 *Physica* C **369** 187
[38] Brandt E H 2001 *Phys. Rev.* B **64** 024505
[39] Orlando T P and Delin K A 1991 *Foundations of Applied Superconductivity* (Reading, MA: Addison-Wesley)
[40] Bleaney B I and Bleaney B 1976 *Electricity and Magnetism* (Oxford: Oxford Science Publications)
[41] Obara H, Kosaka S, Yokoyama Y, Umeda M and Kimura Y 1991 *Phys. Rev.* B **44** 4532
[42] Pleines M, Glückler E M F H, Hofer A, Morenzoni E, Niedemayer C, Prokscha T, Riseman T M, Birke M, Jackson T, Litterst J, Luetkens H, Schatz A and Schatz G 2000 *Physica* B **289–290** 369
[43] Fuchs A, Prusseit W, Berberich P and Kinder H 1996 *Phys. Rev.* B **53** R14745
[44] Sonier J E, Kiefl R F, Brewer J H, Bonn D A, Dunsinger S R, Hardy W N, Liang R, MacFarlane W A and Riseman T M 1997 *Phys. Rev.* B **55** 11789
[45] Thrane B P, Schlenker C, Dumas J and Buder R 1996 *Phys. Rev.* B **54** 15518
[46] Fabbricatore P, Farinon S, Innocenti S and Gömöry F 2000 *Phys. Rev.* B **61** 6413
[47] Zimmermann P, Keller H, Lee S L, Savic I M, Warden M, Zech D, Cubitt R, Forgan E M, Kaldis E, Karpinski J and Krüger C 1995 *Phys. Rev.* B **52** 541